Advanced Journal of Chemistry-Section A, 2020, 3(3), 265–273
Available online at : www.ajchem-a.com
ISSN Online: 2645-5676
DOI: 10.33945/SAMI/AJCA.2020.3.4

Original Research Article

Structural Properties and Cation Distribution in Co^{2+} and Ho^{3+} Ions Induced Nanocrystalline $ZnFe_2O_4$

Jalindhar Gahininath Lohkare[a], Shujat Hussain Quadri[b], Laxamn Appa Dhale[c], Ketankumar Ambadasrao Ganure[d,*]

[a] *Department of Chemistry, Faculty of Science and Technology, S M D M College, Kalamb, Dist. Osmanabad, Maharashtra, India*
[b] *Department of Chemistry, Maulana Azad College, Aurangabad, Dr. Babasaheb Ambedkar Marathwada University, Maharashtra 431004, India*
[c] *Department of Materials Chemistry, Shri Krishna College, Gunjoti, Dr. Babasaheb Ambedkar Marathwada University, Maharashtra 431004, India*
[d] *Department of P. G. Studies and Research in Nanotechnology, Faculty of Science and Technology, Punyashlok Ahilyadevi Holkar Solapur University Solapur-413006, Maharashtra, India*

ARTICLE INFO

Received: 26 July 2019
Revised: 08 August 2019
Accepted: 07 September 2019
Available online: 12 September 2019

KEYWORDS

Nanocrystalline ferrite
Sol-gel auto combustion
X-ray diffraction cation distribution

ABSTRACT

Nanocrystalline $Co_yZn_{1-y}Ho_zFe_{2-z}O_4$ (where y = 0.0, 0.25, 0.5, 0.75, 1.00 and z=0.0, 0.03, 0.06, 0.08, 0.1) ferrites were prepared by sol-gel auto combustion method at pH of 8. Samples were obtained by annealing at relatively low temperature 600 °C for 4 h and characterized by thermo gravimetric/differential thermal analysis (TG/DTA) all the samples were annealed at 600 °C for 4 h. The prepared samples were investigated by X-ray diffraction (XRD), scanning electron microscopy (SEM), transmission electron microscopy (TEM) and Fourier transform infrared (FT-IR) spectroscopy. Particle size measured from XRD and TEM are in good agreement with each other. The TEM study reveals the fine particle nature of the ferrites with little agglomerations. The cation distribution suggests that Zn^{2+} ion mainly on tetrahedral-A sites, Ho^{3+} ions shows strong preference towards octahedral-B site, Co^{2+} and Fe^{3+} ions are randomly distributed at the tetrahedral-A and octahedral-B site. FT-IR study confirmed two main absorption bonds in the frequency range 400-600 cm^{-1}, assigned due to the tetrahedral-A and octahedral-B stretching vibrations.

GRAPHICAL ABSTRACT

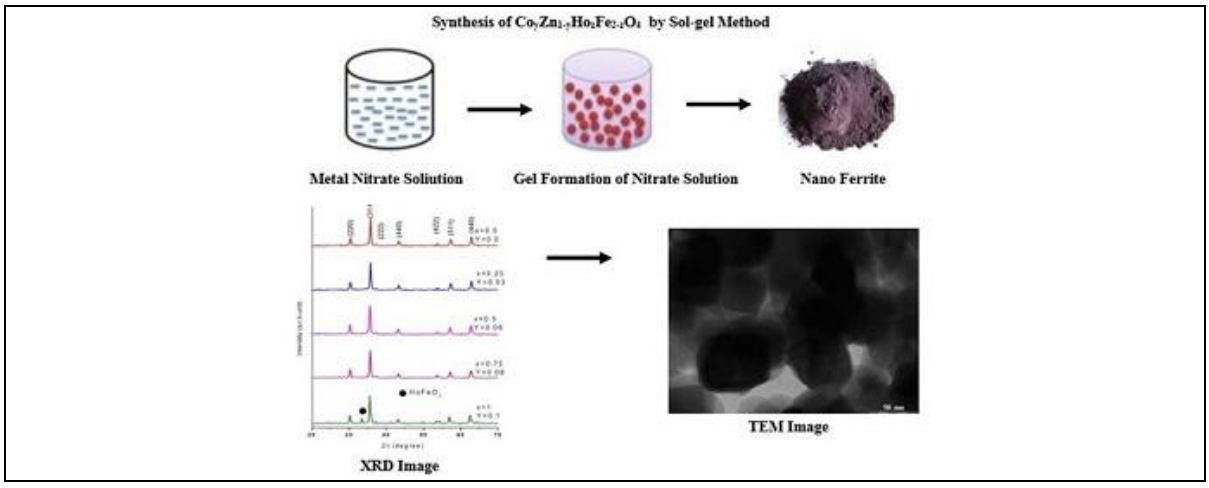

* Corresponding author's E-mail address: ketan.ganure@rediffmail.com

Introduction

Nanocrystalline ferrites play an important role in modern industrial society. Spinel ferrites are technologically attractive due to their promising magnetic properties such as ferro fluids, magnetic drug delivery, high density information storage, *etc.* [1]. Spinel ferrites with a chemical formula $M_{1-y}M'_yFe_{2-z}RE_zO_4$, where M, M' are divalent metals and RE is a rare earth metals respectively can be an attractive material to tailor the structural, electrical and magnetic properties. Application of these kinds of mixed oxides depends on the specific nature of substituting ion, sintering temperature, preparations method *etc*. Generally, rare earth (RE) ions are lies in two categories, one which ionic radius close to iron and second is the ionic radius larger then iron. RE ions have unpaired 4f electrons have a role to originate magnetic anisotropy due to their orbital shape. The magneto crystalline anisotropy in ferrite is related to 4f-3d coupling between transition metal and rare earth ions, therefore doping of rare earth ions into spinel ferrite can be improved by their electric and magnetic properties [2,3]. Zinc ferrite ($ZnFe_2O_4$) is a spinel oxide that possesses excellent magnetic and electrical properties as well as excellent chemical and thermal stabilities. $ZnFe_2O_4$ oxide has received much attention due to its potential applications in detecting gases [4], as an adsorbent material for hot-gas desulfurization [5], in biomedicine [6], for its magnetic, optical and electrical behaviors [7–11] and catalytic application [12,13]. Recently, zinc ferrite has been used as an efficient heterogeneous Fenton catalyst in degrading organic pollutants from an aqueous solution [14-16]. Among the ferrite family, $CoFe_2O_4$ possess excellent magnetic properties, particularly due to the occupation of Co^{2+} ions at octahedral B-site and its large magnetocryslline anisotropy. At the same time, it is observed that RE-Ho^{3+} ions significantly improve the structural and magnetic properties of spinel ferrite [17]. In the present work, reports a study on the effects of Co^{2+}/Ho^{3+} substitution on the structural properties of $ZnFe_2O_4$ ferrite system.

Experimental

Materials and method

Synthesis of nanoparticles

Nanocrystalline powder with a chemical formula $Co_yZn_{1-y}Ho_zFe_{2-z}O_4$ (y=0.0, 0.25, 0.5, 0.75, 1.00 and z=0.0, 0.03, 0.06, 0.08, 0.1) ferrites were prepared by sol-gel auto combustion method. The analytical grade reagent of cobalt nitrate (Co $(NO_3)_2.6H_2O$), zinc nitrate (Zn $(NO_3)_2.6H_2O$), ferric nitrate (Fe $(NO_3)_2.9H_2O$) and holmium nitrate (Ho $(NO_3)_2.6H_2O$), citric acid ($C_6H_8O_7.H_2O$), were used as starting materials. Metal nitrate dissolved in stoichiometric proportion in deionized distilled water, then citric acid solution was added in 1:2 molar ratio, the pH of resulting solution adjusted up to 8, pH by adding aqueous ammonia, then the mixed solution heated on hot plate with continuously stirring at 90 °C, finally as a result of auto combustion, brown colored ash obtained.

Characterization of nanoparticles

The dried powder was characterized via TG/DTA at heating rate of 10 °C/min in air atmosphere to determine the crystallization temperature. A part of the powder was X-ray diffraction method examined on a Rikagu Miniflax II, X-ray diffractometer using Cu-K_α radiation (λ=1.5405Å) radiation. Surface morphology of the powder samples were studies by using scanning electron micrograph (SEM) (Modes-JEOL-JSM-5600N) Transmission electron microscopy (TEM) images of the samples (Model Phillips CM 200), the Fourier transform infrared (FT-IR) spectroscopy of all samples were recorded at room temperature using Perkin Elmer infrared Spectrophotometer.

Results and discussions

TG/DTA

TG and DTA curves of a typical sample $Co_{0.5}Zn_{0.5}Ho_{0.06}Fe_{1.94}O_4$ in the temperature range of 20 to 600 °C are shown in Figure 1 with an increase in temperature. Two stages of weight loss are observed in TGA curve. The weight loss for the Ist stage is attributed due to water vaporization. The exothermic peaks in DTA curve at 356 °C, IInd stage can be attributed to the starting of spinel ferrite crystallization [18], above 500 °C temperature there is no weight loss was observed and the crystallization process was completed, all samples were calcinated at average temperature of ferrite formation at 500 °C.

Elemental analysis

The elemental analysis was carried out to determined elemental composition by EDAX analysis. The obtained results are graphically represented by Figure 2, indicates the theoretical percentages and observed percentages of elements does not match perfectly, because of errors' in preparation techniques and solid state reactions are not stoichiometric reactions.

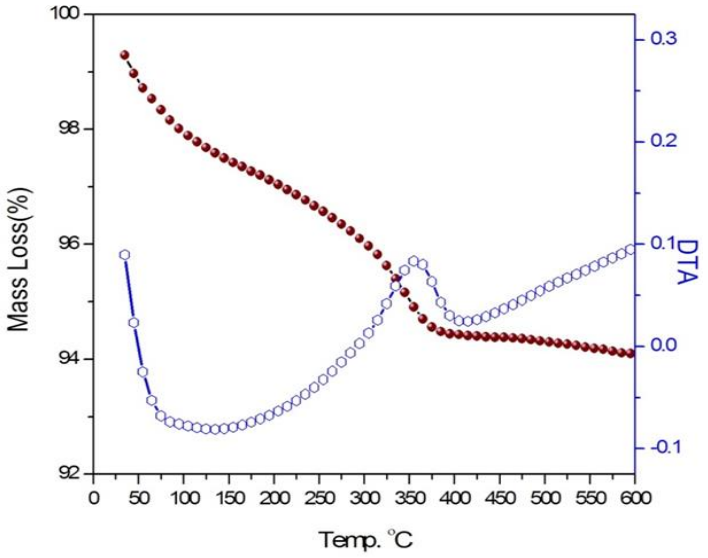

Figure 1. The typical TG/ DTA curve of composition $Co_{0.50}$ $Zn_{0.5}Ho_{0.06}Fe_{1.94}O_4$

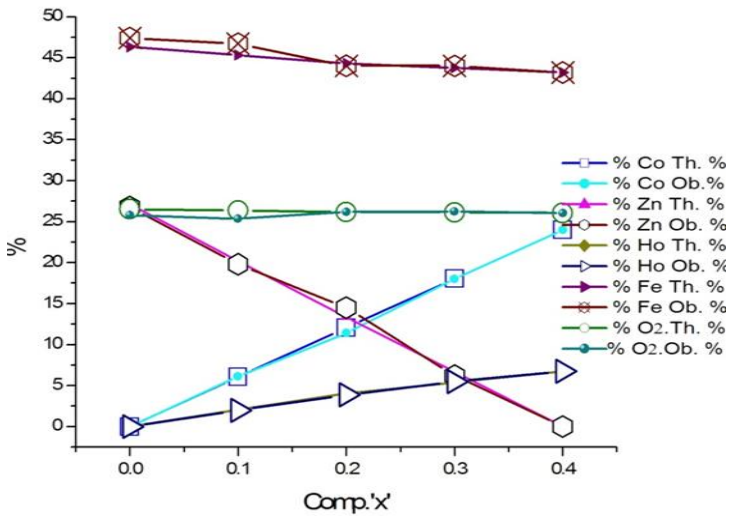

Figure 2. The percentage of element of $Co_yZn_{1-y}Ho_zFe_{2-z}O_4$ (y=0.0, 0.25, 0.5, 0.75, 1.00) and (z=0.0, 0.03, 0.06, 0.08, 0.1)

X-ray analysis

Figure 3 illustrate x-ray diffraction patterns (XRD) of $Co_yZn_{1-y}Ho_zFe_{2-z}O_4$ (y=0.0, 0.25, 0.5, 0.75, 1.00 and z=0.0, 0.03, 0.06, 0.08, 0.1). All the samples show good crystallization, with well-defined diffraction lines. The presence of the strong diffraction peaks corresponding to the planes (220), (311), (222), (400), (422), (511/333), (400), indicates the presence of cubic spinel phase. The peaks are indexed by using JCPS data $ZnFe_2O_4$ (89-1012), $CoFe_2O_4$ (JCPDS.22-1080), and Ho doped ferrite. The weak peak JCPDS corresponding to 2θ (indicated by brownish circle in Figure 3) is attributed to secondary phase at the grain boundaries and appears for z≥0.08 and their intensity increased with the increase of holmium concentration. The crystal lattice is distorted when the defect concentration z is high, that further gives rise to the foundation of the new phase compound. As a result, there was a limit for replacement of Fe^{3+} with Ho^{3+}, therefore, redundant Ho^{3+} ions formed the $HoFeO_3$ on the grain boundaries [17-19].

The lattice constants are determined by using Bragg law as a function of Co^{2+}-Ho^{3+} content addition in Zn ferrites and the values of lattice constant are shown in Table 1. It is observed that the lattice constant decreased with increasing Co^{2+} constant. This probably due to variation of ionic size of Co^{2+} (0.72Å) is lower than that of Zn^{2+} (0.82Å). There is not much of influence on the lattice constant with the substitution of Ho^{3+} ions. This is attributed to fact of the concentration of Ho^{3+} ions that are so small that do not influence the lattice constant and as the Ho^{3+} is high it formed the secondary phase. The lattice constants were found within the range of the lattice constants of $ZnFe_2O_4$ and $CoFe_2O_4$. Average particle sizes 'D_{XRD}' was calculated according to the Debye Scherrer Equation [20]:

$$D_{XRD} = \frac{k\lambda}{\beta \cos\theta} \quad (1)$$

Where, D_{XRD} is the dimension of the crystallites, λ the wavelength of the X-ray radiation, θ the Bragg angle, k is a shape factor taken to be 0.94 and β the peak width measured at half of the maximum intense. The average particles size was obtained by Scherrer's formula and is listed in Table 1, which is found to be in the range of 25-30 nm.

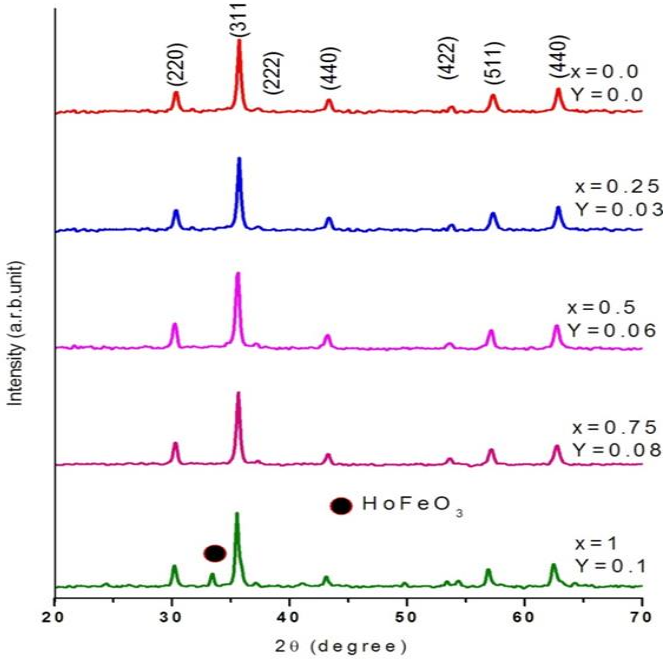

Figure 3. X-ray diffraction patterns of $Co_yZn_{1-y}Ho_zFe_{2-z}O_4$ (y=0.0, 0.25, 0.5, 0.75, 1.00 and (z=0.0, 0.03, 0.06, 0.08, 0.1)

X-ray densities (d_x) of all the investigated samples were calculated from X-ray diffraction analysis and by using the relation [21]:

$$dx = \frac{8M}{Na^3} \quad (2)$$

Where, '8' is the number of molecules per unit cell, 'M' is the molecular weight of sample, 'N' is the Avogadro's number and 'a' is lattice constant. The x-ray density shows increasing trend from 5.4163 to 5.6169 Å, with the increase of Ho^{3+}-Co^{2+} contents. This behavior is mainly depends upon the molecular weight and lattice constant of the samples. The Bulk density 'd_B' was determined by the Archimedes principle using toluene and according to the formula:

$$d_B = (W_s/W_t)\,\rho_t \quad (3)$$

Where, W_s denotes weights of the specimen in air, W_t is the apparent weight loss in toluene and ρ_t is the density of toluene= 0.857 g/cc. The Bulks density of samples varies from 2.77-3.17 with the substitution of Ho^{3+}-Co^{2+} ions. Percentage porosity (P %) of the investigated ferrite samples is determined by employing the relations [21]:

$$P = \left(\frac{d_X - d_B}{d_X}\right) \times 100 \quad (4)$$

Where, d_x and d_B are the X-ray density and bulk density respectively. The percentage porosity observed from 42.65 to 50.24% with Ho^{3+}-Co^{2+} doping concentration y and z. The values of the percentage porosity are given in Table 1. Hopping lengths (L_A, L_B) between magnetic ions (the distance between the ions) in the tetrahedral (A) site and octahedral [B] site can be calculated using the relation discussed elsewhere [22]. The values of hopping length are given in Table 1. This shows that hopping length decreased with increasing Co^{2+}-Ho^{3+} concentration.

Table 1. Composition, secondary phase, lattice constant ('an' observed and theoretical), X-ray density (d_x), bulk density (d_B), Percentage Porosity (P), Particle size (D_{XRD} and D_{TEM}), and Hopping lengths (L_A and L_B) of $Co_yZn_{1-y}Ho_zFe_{2-z}O_4$. (y=0.0, 0.25, 0.5, 0.75, 1.00) and (z=0.0, 0.03, 0.06, 0.08, 0.1)

Compositions	Phase	a(obs.) (Å)	$a_{(Theo.)}$ (Å)	Dx (Å)	d_B (g/cm³)	P (%)	D_{XRD} (nm)	D_{TEM} (nm)	L_A (Å)	L_B (Å)
$Co_{0.0}Zn_{1.0}Ho_{0.0}Fe_2O_4$.	-	8.393	8.478	5.416	2.801	48.2	25.49	26.2	3.634	2.967
$Co_{0.25}$	-	8.375	8.483	5.488	3.147	42.6	29.58	30.1	3.626	2.961
$Zn_{0.75}Ho_{0.03}Fe_{1.97}O_4$.										
$Co_{0.50}$	-							26.8		
$Zn_{0.5}Ho_{0.06}Fe_{1.94}O_4$		8.362	8.489	5.550	3.178	42.7	25.35		3.621	2.956
$Co_{0.75}$	$HoFeO_3$							27.5		
$Zn_{0.25}Ho_{0.08}Fe_{1.92}O_4$		8.351	8.492	5.585	2.779	50.2	29.59		3.616	2.952
$Co_{1.0}Zn_0Ho_{0.1}Fe_{1.90}O_4$	$HoFeO_3$	8.342	8.495	5.616	2.864	49.0	27.71	28.1	3.612	2.949

Cation distribution

The cation distributions were obtained from the analysis of intensity of X-rays diffraction patterns. In this method, the observed intensity ratio was compared with the calculated intensity ratio. Bertaut method [23] was used to determine the cation distributions. In this method selects a few pairs of reflections in accordance to the expression:

$$\frac{I_{hkl}^{obs}}{I_{h'k'l'}^{obs}} = \frac{I_{hkl}^{cal}}{I_{h'k'l'}^{cal}} \quad (5)$$

Where, I_{hkl}^{obs} are I_{hkl}^{cal} the observed and calculated intensities for the reflection (hkl) respectively.

The best information on the cation distribution are achieved by comparing the calculated and observed intensity ratios for reflections, whose intensities are nearly

independent of the oxygen parameters. In the present system the reflections of (400), (400), (420) and (422) were used to calculate the intensity ratio. These planes are assumed to be sensitive to the cation distributions. The temperature of absorption factors is not taken into account in our calculations as they do not affect the intensity calculation. the agreement factor 'R' best simulated structure which matches the actual structure of the sample will lead to a minimum value of 'R' and the corresponding cation distribution is obtained for each (hkl) and reflection pair considered:

$$R = \frac{I_{hkl}^{obs}}{I_{h'k'l'}^{obs}} - \frac{I_{hkl}^{cal}}{I_{h'k'l'}^{cal}} \quad (6)$$

The calculation of the relative integrated intensity (I_{hkl}) of a given diffraction line from powder specimens as observed in a diffractometer with a flat-plate sample holder. The following formula is valid:

$$I_{hkl} = [F]_{hkl}^2 P.L_P \quad (7)$$

Where, F is the structure factor, P is multiplicity factor, L_P is the Lorentz–polarization factor and

$$L_P = \frac{1+Cos^2 2\theta}{Sin^2\theta Cos\theta} \quad (8)$$

The atomic scattering factors for various ions are taken from the literature [20]. The cation distribution for the presently investigated spinel ferrite system $Co_yZn_{1-y}Ho_zFe_{2-z}O_4$ (y=0.0, 0.25, 0.5, 0.75, 1.00) and (z=0.0, 0.03, 0.06, 0.08, 0.1) was obtained from the X-ray diffraction technique and are presented in Table 2. The cation distribution for each concentration and the site preferences of the cations distributes among tetrahedral (A) site and octahedral [B] site showing the fraction of Fe^{3+} ions on either site. The $ZnFe_2O_4$ has a normal cubic spinel structure where Zn^{2+} ions are mainly residing at (A) sites and Fe^{3+} ions distributed among the [B] sites. The cation distribution is presented in Table 2. Indicate that Ho^{3+} ions occupy the octahedral [B] sites, which is consist with their preference to octahedral [B] sites. Further, this occupation increased with Ho^{3+} content, the fraction of Fe^{3+} ions octahedral sites decreases linearly and on the other hand Co^{2+} concentration increases.

Table 2. Composition, Cation distribution, Intensity ratio (calculate and observe) and agreement factor (R) of $Co_yZn_{1-y}Ho_zFe_{2-z}O_4$. (y=0.0, 0.25, 0.5, 0.75, 1.00) and (z=0.0, 0.03, 0.06, 0.08, 0.1)

Compositions	Cation distribution		Intensity Ratio 400/440		Intensity Ratio 440/422			Agreement factor (R)
	(A Site)	[B site]	Cal	Obs	Cal	Obs		
$Co_{0.0}Zn_{1.0}Ho_{0.0}Fe_2O_4$.	$(Zn_1)^A$	$[Fe_2]^B$	0.347	0.436	3.63	4.996	0.088	1.364
$Co_{0.25}Zn_{0.75}Ho_{0.03}Fe_{1.97}O_4$	$(Zn_{0.75}Fe_{0.25})^A$	$[Co_{0.25}Ho_{0.03}Fe_{1.72}]^B$	0.382	0.444	4.04	4.937	0.061	0.897
$Co_{0.50}Zn_{0.5}Ho_{0.06}Fe_{1.94}O_4$	$(Co_{0.05}Zn_{0.5}Fe_{0.45})^A$	$[Co_{0.45}Ho_{0.06}Fe_{1.49}]^B$	0.422	0.509	4.44	4.403	0.087	-0.037
$Co_{0.75}Zn_{0.25}Ho_{0.08}Fe_{1.92}O_4$	$(Co_{0.1}Zn_{0.25}Fe_{0.65})^A$	$[Co_{0.65}Ho_{0.08}Fe_{1.27}]^B$	0.459	0.487	4.79	4.543	0.028	-0.247
$Co_{1.0}Zn_0Ho_{0.1}Fe_{1.90}O_4$	$(Co_{0.15}Fe_{0.85})^A$ [Co_{085}	$Ho_{0.1}Fe_{1.05}]^B$	0.496	0.490	5.28	4.414	-0.006	-0.874

Fourier transformed infrared spectroscopy (FT-IR)

Fourier transformed infrared spectra of as obtained ferrite nanoparticles measured in the frequency range of 200-800 cm^{-1} is shown in Figure 5. The two absorption bands υ_1 and υ_2 are observed at a lower frequency range corresponding to 557 to 599 and 410 to 454 cm^{-1} wave number respectively. These bands are important characteristics peaks of spinel ferrites [24,25]. The force constants corresponding to the tetrahedral and octahedral complexes are calculated by using the standard formulae given below [26].

$$K_T = 7.62 \times m_1 \times \upsilon_1^2 \times 10^{-2} \quad (9)$$

$$K_O = 10.62 \times \frac{m_2}{2} \times \upsilon_2^2 \times 10^{-2} \quad (10)$$

Where, K_T is the force constant of tetrahedral (A) site and K_O is the force constant of octahedral [B] site, M_1 molecular weight of tetrahedral (A) site, M_2 molecular weight of octahedral [B] site, υ_1 and υ_2 are corresponding center frequency on tetrahedral site and octahedral site respectively. The force constant K_T and K_O values are tabulated in Table 3.

SEM analysis

SEM micrographs were used to obtain further structural information. The micrographs show good spherical shaped particles in the material. The micrographs also indicate nearly uniform distribution of particles, better grain boundaries were observed at Ho^{3+}/Co^{2+} ions. The scanning electron micrograph for the typical samples $Co_{0.5}Zn_{0.5}Ho_{0.06}Fe_{1.94}O_4$ and $Co_{0.75}Zn_{0.25}Ho_{0.08}Fe_{1.92}O_4$ are shown in Figure 5 (a) and (b).

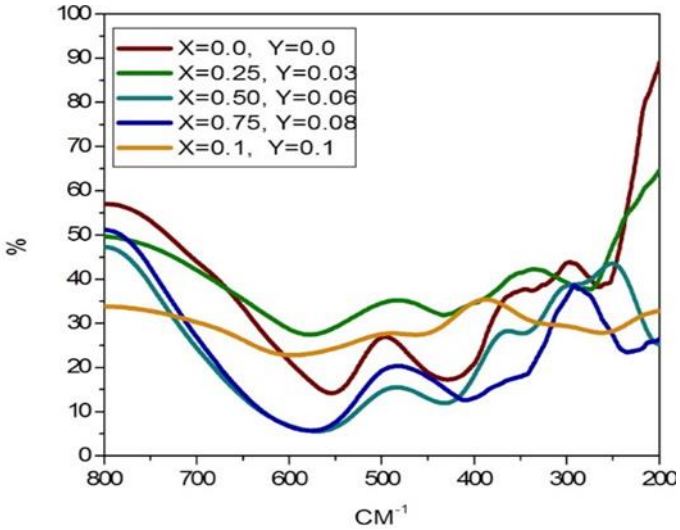

Figure 4. FT-IR pattern of $Co_yZn_{1-y}Ho_z Fe_{2-z}O_4$ (y=0.0, 0.25, 0.5, 0.75, 1.00 and (z=0.0, 0.03, 0.06, 0.08, 0.1)

Table 3. Composition values, wave number (υ_1, υ_2), force constant (K_0 and K_t) of $Co_yZn_{1-y}Ho_zFe_{2-z}O_4$. (y=0.0, 0.25, 0.5, 0.75, 1.00 and z=0.0, 0.03, 0.06, 0.08, 0.1)

Compositions	υ_1 (cm^{-1})	υ_2 (cm^{-1})	K_0 (dyne/cm)	K_t (dyne/cm)
$Co_{0.0}Zn_1Ho_{0.0}Fe_2O_4$	557.43	424.34	113914	190654
$Co_{0.25}Zn_{0.75}Ho_{0.03}Fe_{1.97}O_4$	571.92	435.91	118730	199875
$Co_{0.50}Zn_{0.5}Ho_{0.06}Fe_{1.94}O_4$	568.04	428.22	113174	192022
$Co_{0.75}Zn_{0.25}Ho_{0.08}Fe_{1.92}O_4$	571.72	410.91	102853	176843
$Co_{1.0}Zn_0Ho_{0.1}Fe_{1.90}O_4$	599.87	454.24	123947	211910

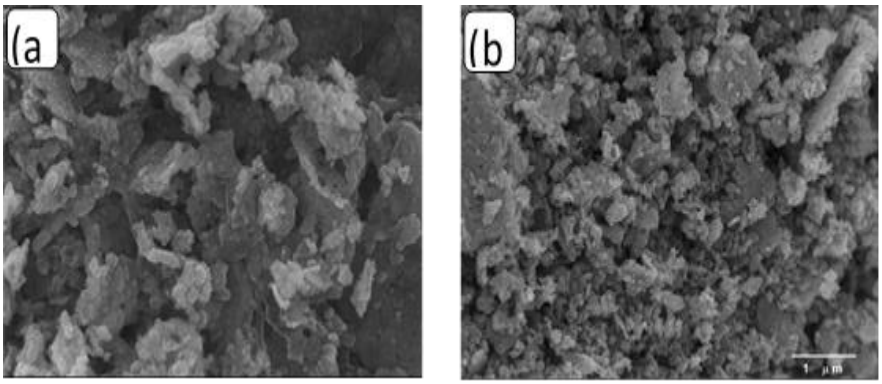

Figure 5. (a) SEM image of $Co_{0.5}Zn_{0.5}Ho_{0.06}Fe_{1.94}O_4$ (b) SEM image of $Co_{0.75}Zn_{0.25}Ho_{0.08}Fe_{1.92}O_4$.

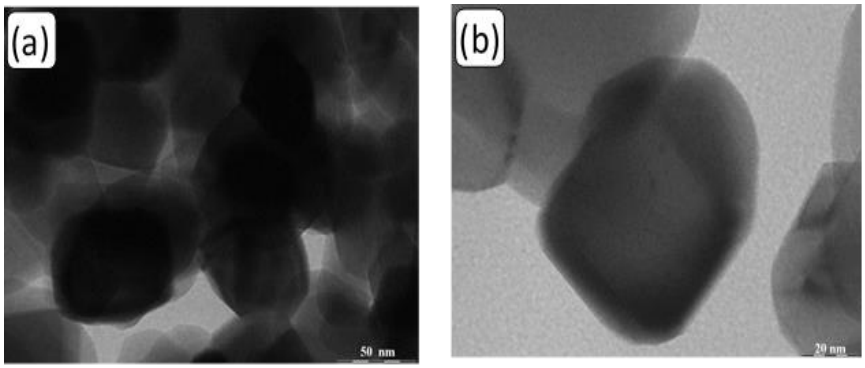

Figure 6. (a) TEM image of $Co_{0.5}Zn_{0.5}Ho_{0.06}Fe_{1.94}O_4$, (b) TEM image of $Co_{0.75}Zn_{0.25}Ho_{0.08}Fe_{1.92}O_4$

TEM analysis

The size and morphology of the synthesized nanoparticles of $Co_{0.5}Zn_{0.5}Ho_{0.06}Fe_{1.94}O_4$ and $Co_{0.75}Zn_{0.25}Ho_{0.08}Fe_{1.92}O_4$ were observed by transmission electron microscopy (TEM) and is present in Figures 6 (a and b). The particles size is lies in the range of 26-30 nm. The calculated crystalline size (D_{XRD}) is in good agreement with that observed from transmission electron microscopy.

Conclusion

A simple sol–gel auto combustion process using citric acid was employed to synthesize the $Co_yZn_{1-y}Ho_zFe_{2-z}O_4$ (y=0.0, 0.25, 0.5, 0.75, 1.00) and (z=0.0, 0.03, 0.06, 0.08, 0.10) ferrite nanoparticles. Average crystalline size calculated from XRD data was found in nano range. The unit cell parameter 'a' decreases linearly with increases Co^{2+}-Ho^{3+} concentration. All the samples doped with Ho^{3+} ion contained mainly ferrite spinal phase in combination of a small amount of a foreign $HoFeO_3$ phase observed. The scanning electron microscopy micrographs show the agglomerated grainy structure. Cation distribution estimated from Bertaut method indicates that Co and Ho ions show marked preference towards octahedral B-site, whereas Zn ions occupy tetrahedral A-site only. Fe ions are distributed randomly over both the available sites. FT-IR study confirms two main metal-oxygen bands at ~600 cm^{-1} and ~430 cm^{-1} corresponding to the vibrations of the tetrahedral and octahedral M-O bond respectively. The particle size measured by both XRD and TEM are in very good agreement with each other and that the size distribution of the prepared nanoparticles is small.

Acknowledgments

The authors Dr. Ketankuma A Ganure, Jalindhar Lohkare, Laxamn A Dhale and Quadri S Hussain are thankful to TIFR Mumbai, for providing the SEM facility, Shivaji University, Kholapur for providing the TGA/DSC facility, IIT Mumbai for providing TEM facility and Special

Thanks to Research Center Maulana Azad College for providing the research Facility.

Disclosure statement

No potential conflict of interest was reported by the authors.

ORCID

Ketankumar A. Ganure : 0000-0002-1119-7641

References

[1] R.D.K. Misra, A. Kale, R.S. Srivastav, O.N. Senkov, *Mater. Sci. Technol.,* **2003,** 19, 826–830.
[2] P.K. Roy, B. Nayak, J. Bera, *J. Magn. Magn. Mater.,* **2008**, *320*, 1128–1132.
[3] Y.M Al Angari, J. Magn. Magn. Mater., **2011**, *323*, 1835–1839.
[4] X. Chu, X. Liu, G. Meng, *Sens. Actuat. B Chem.,* **1999**, *55*, 19–22.
[5] M.A. Ahmed, L. Alonso, J.M. Palacios, C. Cilleruelo, J.C. Abanades, *Solid State Ion.,* **2000,** *138*, 51–62.
[6] J. Wan, X. Jiang, H. Li, K. Chen, *J. Mater. Chem.,* **2012**, *22*, 13500–13505.
[7] A. Albuquerque, J.D. Ardisson, E. Bittencourt, W.A.A. Macedo, *Mater. Res.,* **1999**, *2*, 235–238.
[8] G.Y. Kumar, H.B. Naik, A.S. Roy, K.N. Harish, R. Viswanath, *Nanomater. Nanotechnol.,* **2012**, *2*, 19.
[9] A. Mekap, P.R. Das, R.N.P. Choudhary, *J. Mater. Sci. Mater. Electron.,* **2013**, *24*, 4757–4763.
[10] A.M. Gama, M.C. Rezende, *Mater. Res.,* **2013**, *16*, 997–1001.
[11] O.V. Yelenich, S.O. Solopan, T.V. Kolodiazhnyi, V.V. Dzyublyuk, A.I. Tovstolytkin, A.G. *Mater. Chem. Phys.*, **2014**, *146*, 129–135.
[12] J.A. Toledo-Antonio, N. Nava, M. Martinez, X. Bokhimi, *Appl. Catal. A Gen.,* **2002**, *234*, 137–144.
[13] E. Casbeer, V.K. Sharma, X.Z. Li, *Sep. Purif. Technol.,* **2012**, *87*, 1–14.
[14] L. Liu, G. Zhang, L. Wang, T. Huang, L. Qin, *Ind. Eng. Chem. Res.,* **2011**, *50*, 7219–7227.
[15] P. Li, H.Y. Xu, X. Li, W.C. Liu, Y. Li, *Adv. Mater. Res.,* **2012**, *550*, 329–335.
[16] J. Wu, W. Pu, C. Yang, M. Zhang, J. Zhang, *J. Environ. Sci.,* **2013**, *25*, 801–807.
[17] S.E. Shirsath, M.L. Mane, Y. Yasukawa, X. Liu, A. Morisako, *Phys. Chem. Chem. Phys.,* **2014**, *16*, 2347–2357.
[18] M.A Gabal, Y.M Al Angari, *Mater. Chem. Phys.,* **2009**, *115*, 578–584.
[19] K. Kamala Bharti, G. Markandeyulu, C.V. Ramana, *J. Phys. Chem. C,* **2010**, *115*, 554–560.
[20] B.D. Cullity. *Elements of X-ray diffraction*, Addision-Wesley, London, **1959**.
[21] Vivek Chaudhari, S.E. Shirsath, M.L. Mane, R.H. Kadam, S.B. Shelke, D.R. Mane., *J. Alloy. Compd.,* **2013**, *549*, 213–220.
[22] T. Abbas, Y. Khan, M. Ahmad, J. Solid State Commun., **1992,** *82*, 701–703.
[23] L. Weil, F. Bertaut, L. Bochirol, *J. Phys. Radium*, **1950**, *11*, 208–212.
[24] A.M. Shaikh, S.A. Jadhav, S.C. Watwe, B. K. Chougule, *Mater. Lett.,* **2000**, *44*, 192–196.
[25] H.M. Kazi, S.F. Mansour, *J. Phys. Chem. Solid.,* **2006**, *67*, 1643–1648.
[26] R.D. Waldron, *Phys. Rev.,* **1955**, *99*, 1727.

How to cite this manuscript: Jalindhar Lohakre, Qudari S. Hussain, Laxman A. Dhale, Ketankumar A. Ganure, Structural Properties and Cation Distribution in Co^{2+} and Ho^{3+} Ions Induced Nanocrystalline $ZnFe_2O_4$, *Adv. J. Chem. A*, **2020**, *3*(3), 265–273.